Acta Crystallographica Section D
Biological Crystallography
ISSN 0907-4449

Accurate rocking-curve measurements on protein crystals grown in a homogeneous magnetic field of 2.4 T

Daniel Lübbert,* Alke Meents and Edgar Weckert

HASYLAB/DESY, Notkestrasse 85, D-22607 Hamburg, Germany

Correspondence e-mail: daniel.luebbert@desy.de

Received 8 December 2003
Accepted 8 March 2004

Differences in mosaicity between lysozyme crystals grown inside and outside a homogeneous magnetic field of 2.4 T and with and without agarose gel were investigated by X-ray diffraction rocking-curve measurements. High angular resolution was achieved using an Si(113) four-reflection Bartels monochromator. The results show that (i) all crystals were highly perfect, (ii) the mosaicities were clearly anisotropic and (iii) the mosaicities varied more strongly within each group of crystals (grown under identical conditions) than the average values across groups. In particular, the effect of the magnetic field on crystal mosaicity was found to be very small. Finally, the spatial distribution of mosaic blocks inside a protein crystal was visualized with a novel diffraction technique using a high spatial resolution two-dimensional CCD detector.

1. Introduction

In order to understand the physiological functions of many protein molecules on a structural basis high-resolution crystal structure data are necessary, which in many cases are easier to measure accurately from crystals of lower mosaicity. In addition to the usual crystal-quality optimization procedures *via* salt concentration, temperature control *etc*., a number of additional methods have been applied in recent years, such as crystal growth in microgravity, in gels and in magnetic fields. In this paper, we study crystals grown in gels and magnetic fields.

The usefulness of gels in the crystallization of small and inorganic compounds has been known for a long time (Henisch, 1988). The first applications of gels to the growth of protein crystals were reported over a decade ago (Robert & Lefaucheux, 1988; Provost & Robert, 1991; Miller *et al.*, 1992). A beneficial influence on the growth properties was expected from the fact that gels reduce convection in the growth medium, prevent sedimentation, suppress nucleation and reduce twinning (Thiessen, 1994; Biertümpfel *et al.*, 2002). In this sense, growth in gels can mimic the influence of microgravity and has been suggested as a substitute for or for use in combination with growth in space. Different types of gelling agents and different methods for the gel growth of protein crystals have subsequently been applied (Garcia-Ruiz & Moreno, 1994; Cudney *et al*., 1994; Lorber *et al.*, 1999; López-Jaramillo *et al.*, 2001; Zhu *et al.*, 2001; Garcia-Ruiz *et al.*, 2002). The main experimental findings were that crystals grew to larger sizes in gels and that their lattice quality, although not significantly better, appeared to be more uniform (Lorber *et al.*, 1999; Vidal *et al.*, 1999). X-ray studies, which are often limited to individual or small numbers of crystals, showed that gel-grown crystals had smaller mosaicities (Vidal *et al.*, 1999) and a better intensity data resolution limit (Dong *et al.*, 1999) than solution-grown control groups. The latter effect may

indicate a higher lattice quality, but may also simply be a consequence of the larger average crystal volume of gel-grown crystals.

It has been predicted that protein molecules containing α-helices exhibit an anisotropic diamagnetic susceptibility (Pauling, 1936; Worcester, 1978). This leads to an orientational alignment of protein crystals grown in a magnetic field, which has been observed experimentally in recent investigations by various groups (Astier *et al.*, 1998; Sakurazawa *et al.*, 1999; Yanagiya *et al.*, 1999), mainly using optical microscopy. In the specific case of tetragonal lysozyme crystals, the *c* axis was found to be aligned along the magnetic field direction (Ataka *et al.*, 1997). In a series of studies, Wakayama and coworkers (Lin *et al.*, 2000; Ataka & Wakayama, 2002) discussed potential further effects of a homogeneous magnetic field on crystal growth: damping of convection in the growth medium arising from a magnetically induced increase in viscosity (Zhong & Wakayama, 2001), reduced growth rates and decreased diffusion coefficients of protein solutions in a magnetic field (Yin *et al.*, 2002). In an inhomogeneous magnetic field of sufficient strength, diamagnetic levitation of protein crystals will occur (Wakayama *et al.*, 1997), also leading to reduced convection similar to the case of microgravity (Qi *et al.*, 1999, 2001). Again using optical microscopy, a reduced nucleation and growth rate was observed in magnetic fields (Sazaki *et al.*, 1997; Yanagiya *et al.*, 2000). Compared with the case without magnetic field, these effects lead to slower growth of a smaller number of larger crystals, which are expected to have a more perfect crystal lattice and higher diffraction power, thereby facilitating high-resolution structure determination.

Only a few studies have been published to date that report X-ray diffraction experiments on protein crystals grown in a magnetic field in order to test these expectations (Lin *et al.*, 2000; Sato *et al.*, 2001). It appears that no unique method of comparing the crystal quality of protein crystals grown by different methods has been established in the literature so far. Possible criteria include the intensity data-resolution limit and the angular width of X-ray diffraction rocking curves. Among the techniques used in the literature are the fine-slicing method (Bellamy *et al.*, 2000; Borgstahl *et al.*, 2001) and combinations of X-ray diffractometry and topography (see, for example, Boggon *et al.*, 2000). In the present work, we propose a method based on X-ray rocking-curve measurements and statistical data analysis to systematically compare the diffraction properties of a series of protein crystals and apply it to study the effects of both gel and magnetic field on protein crystal growth.

The resolution limit defines the total information content of an experimental data set. All efforts to improve crystal quality target this quantity. However, its experimental value also depends on the incident X-ray flux, background scattering, detector noise and other factors that cannot be precisely controlled and kept constant, especially when results from different experimental stations are to be compared.

An alternative measure of crystalline quality and homogeneity is the crystal mosaicity, which can be experimentally determined *via* the width of X-ray diffraction rocking curves. Even though the interrelation between mosaicity and resolution limit remains an interesting topic of discussion, the mosaicity determined in this way is an experimental quantity than can be more easily compared between experiments. The rocking-curve width can be measured with high precision and reproducibility and depends only on the sample properties, apart from the known divergence and wavelength spread of the incident beam.

Table 1
Numbers of samples used in this study that were grown with/without magnetic field and with/without gel.

	Without gel	With gel	Total
B = 0 T	6	6	12
B = 2.4 T	4	6	10
Total	10	12	22

Table 2
Numbers of rocking curves collected from samples grown with/without magnetic field and with/without gel.

	Without gel	With gel	Total
B = 0 T	72	72	144
B = 2.4 T	47	72	119
Total	119	144	263

Rocking-curve measurements have been used in previous studies to investigate the effect of microgravity growth on crystal quality in the case of lysozyme (Snell *et al.*, 1995) and apocrustacyanin C_1 (Snell *et al.*, 1997). In this article, we present results obtained with a newly developed instrumental setup that allows measurement of rocking curves with very high angular precision. Using this setup, we perform a comprehensive series of rocking-curve measurements in order to investigate the effect of growth in a homogeneous magnetic field of 2.4 T on crystal quality. In parallel, we apply the same comparison technique to crystals grown in gel, a method which is also thought to lead to improved crystal quality (Lorber *et al.*, 1999; Vidal *et al.*, 1999). In this first investigation, hen egg-white lysozyme (HEWL) is used as an exemplary model substance. While the structure and crystallization conditions of this protein are already well known, the methodology developed in this study is applicable to any kind of protein.

2. Experimental procedure

2.1. Samples and crystal-growth conditions

Lysozyme was purchased from Sigma–Aldrich Co. and used without further purification. Prior to crystallization, all solutions were filtered through 0.22 µm filters. Crystals of tetragonal lysozyme were grown by hanging-drop vapour diffusion: equal volumes of protein solution (52 mg ml^{-1}) and 6%(*w*/*v*) NaCl in 0.13 *M* sodium acetate pH 5.3 were mixed and the droplets were equilibrated against a solution containing 6%(*w*/*v*) NaCl. In the case of gel crystallization, the droplets additionally contained 0.3% agarose.

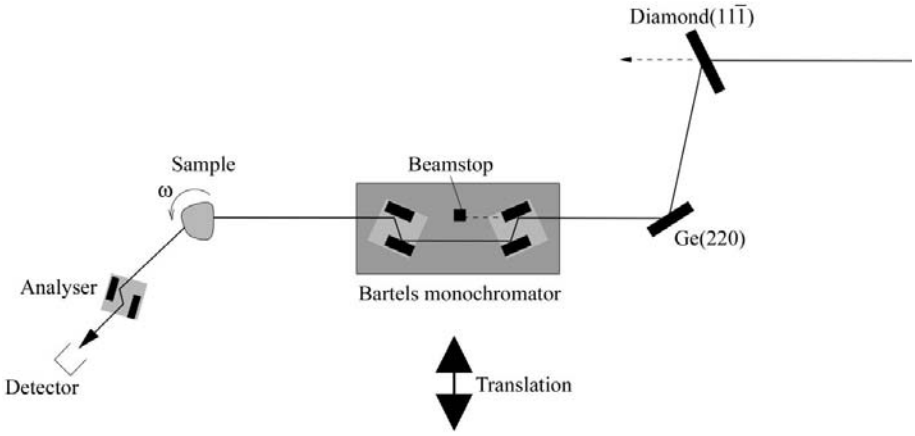

Figure 1
Sketch of the beamline geometry. The Bartels monochromator as well as the channel-cut analyzer crystal were mobile and could be inserted or removed from the beam path as necessary. The analyzer was used exclusively to record the reciprocal-space map (Fig. 4). Note that Bragg angles are not drawn to scale. For further explanations see main text.

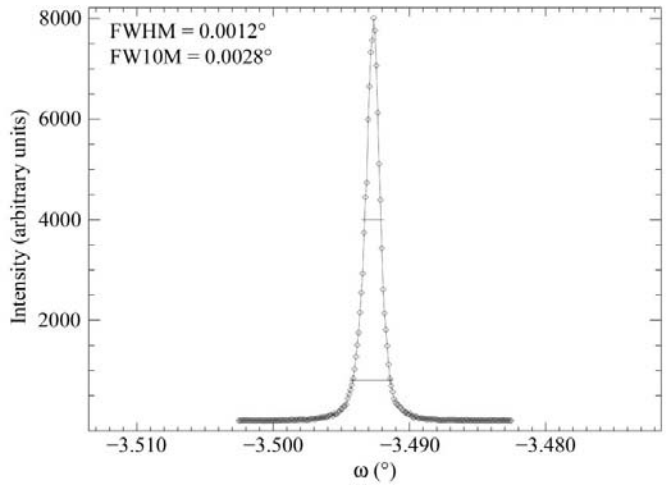

Figure 2
Example of a very narrow rocking curve measured on the (008) reflection of a lysozyme crystal grown with gel and in a magnetic field. Horizontal bars show the full-width at half-maximum (FWHM) of 0.0012° and the full width at 10% of the maximum (FW10M) of 0.0028°. The very low width of this curve simultaneously demonstrates the high crystalline perfection of the sample and the high angular resolution of the instrumental setup. Only about 5×10^{-5} ° of the measured FWHM value arises from the instrumental resolution of the setup (see equation 1). Note that the relative angular scales in all plots of Figs. 2–5 are identical.

Half of the crystallization vessels were placed for 7 d in the 12 mm gap of a Brucker CE-45 electromagnet providing a spatially homogeneous magnetic field of 2.4 T. For these as well as for the control group without magnetic field, the temperature in the crystallization region was held constant at room temperature (293 K) to within ±0.1 K.

2.2. X-ray diffractometry

X-ray diffraction experiments were carried out at the PETRA-1 undulator beamline of DESY, Hamburg (Germany). The optical elements of the beamline are summarized in Fig. 1. A two-crystal monochromator consisting of a diamond(11$\bar{1}$) crystal in Laue (transmission) geometry and a germanium(220) crystal in Bragg (reflection) geometry was used to select an X-ray wavelength of $\lambda = 0.577$ Å (photon energy 21.5 keV). In addition, a high-resolution Bartels monochromator, consisting of two Si(113) channel-cut crystals mounted on a translation stage, could optionally be inserted into the beam path. The purpose of this device was to further reduce the divergence and wavelength spread of the incident X-ray beam in order to reach a higher angular resolution in the rocking-curve measurements. From a DuMond diagram calculation, the combination of both monochromators is expected to provide a relative wavelength spread of $\Delta\lambda/\lambda = 1.7 \times 10^{-5}$ and a divergence of 0.00032° (1 arcsec) for the incident X-ray beam used to carry out the high-resolution rocking-curve measurements.

Samples were placed on a six-circle diffractometer with high mechanical accuracy (minimum angular step width 5×10^{-5} °; Weckert & Hümmer, 1997). A horizontal scattering geometry was chosen for both the monochromator and the sample. The instrument was equipped with two point detectors [NaI(Tl) and plastic scintillator] and a 165 mm diameter MAR CCD area detector. When using the point detector, an optional channel-cut Si(113) analyzer crystal could be inserted into the diffracted beam path in order to obtain higher angular resolution for the exit angle. A more detailed account of the experimental setup will follow (Meents *et al.*, 2004).

The orientation matrix of each crystal was derived from a series of 20–30 two-dimensional rotation diffraction patterns using the *XDS* software package (Kabsch, 2001). The exposure time was kept to a minimum in order to minimize radiation damage. The orientation matrix obtained in this way was accurate enough to find reflections with a point detector.

Rocking curves were measured by recording profiles of scattered X-ray intensity with a point detector while rotating the reciprocal-lattice vector across the Ewald sphere around the vertical ω rotation axis (Fig. 1). The total angular range covered was 0.02–0.04°. This procedure was repeated for several different azimuth angle settings for each crystal, making use of the Ψ degree of freedom of the six-circle diffractometer (Snell *et al.*, 1995). In this way, and by investigating several complementary Bragg reflections, a comprehensive picture of the anisotropic mosaicity of each crystal could be obtained. A total of 12 rocking curves were measured on each crystal, at azimuth angles −45, 0 and 45° for the (16 16 0), the (16 $\bar{16}$ 0), the (008) and the (776) reflections, corresponding to a resolution of 3.47, 3.47, 4.72 and 4.93 Å, respectively. A series of 22 lysozyme crystals were investigated with an identical experimental procedure, yielding a final data set of 263 rocking curves. The numbers of crystals and of

rocking curves per category (grown inside/outside the magnetic field and with/without gel) are summarized in Tables 1 and 2.

3. Results

Selected experimental rocking curves are shown in Figs. 2 and 3. Fig. 2 is an example of a narrow nearly Gaussian curve, having a full-width at half-maximum (FWHM) of 0.0012° (4.3 arcsec). Previous rocking-curve studies on lysozyme crystals found FWHM values mostly in the range 0.005–0.012°, with occasional cases of curves as narrow as 0.002–0.003° (Snell *et al.*, 1995). To our knowledge, the very low value found here is among the lowest values documented in the literature and thus demonstrates simultaneously the very good angular resolution of the instrumental setup and the highly perfect crystalline lattice of the sample.

Several examples of wider rocking curves from less perfect crystals are shown in Fig. 3. These curves display various kinds of deviations from the ideal narrow Gaussian profile, such as double and triple peaks or a continuous plateau of side peaks. Side peaks in the rocking curve are generated by single crystallites (mosaic blocks), the crystal lattices of which have a slightly different orientation than the main part of the sample.

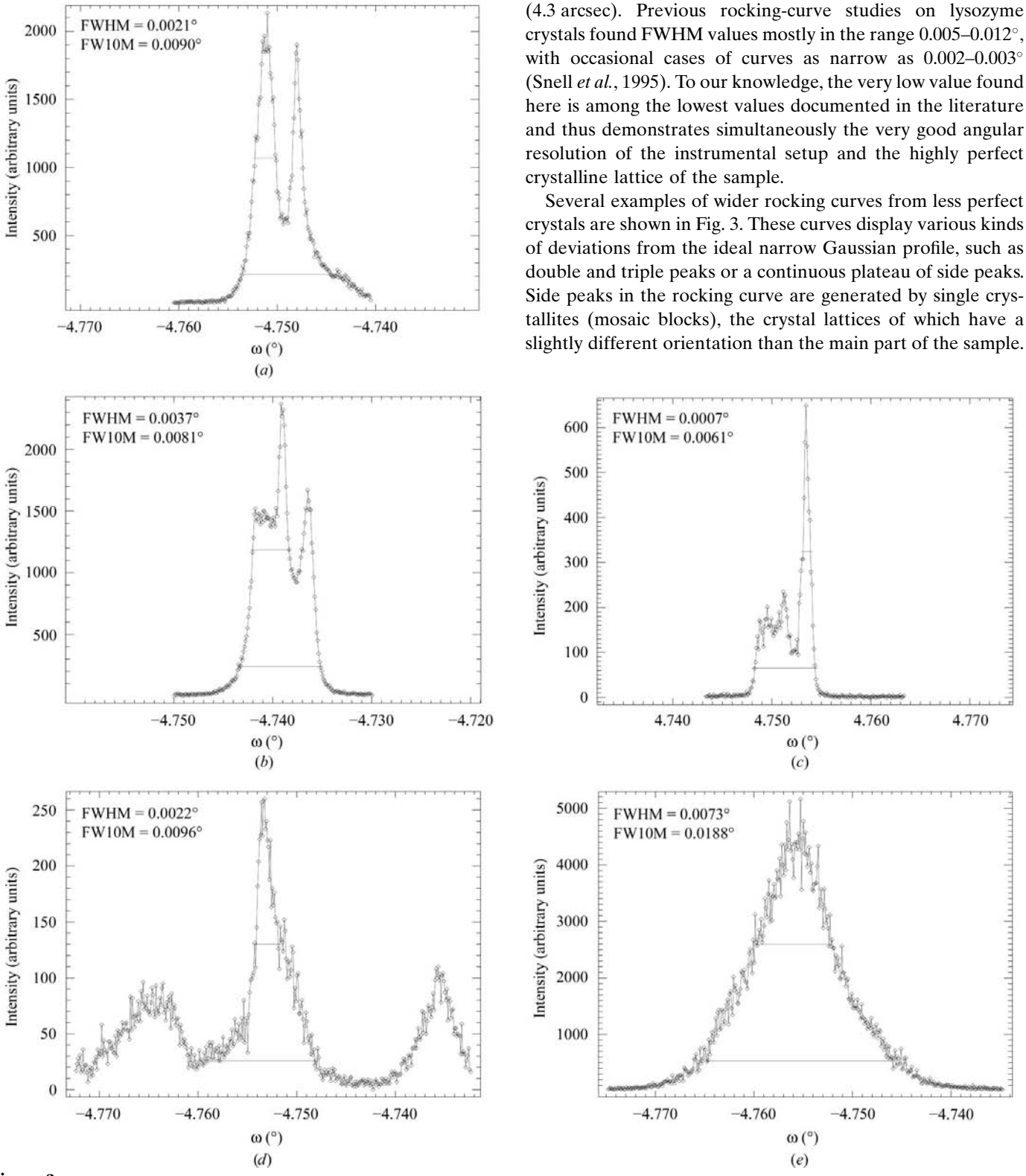

Figure 3
Examples of rocking curves from less perfect crystals showing either two separate peaks or one narrow main peak plus broad tails. All curves were measured on the (16 16 0) [or (16 $\overline{16}$ 0)] reflection of tetragonal lysozyme crystals grown under the following conditions: (*a*) and (*b*) B = 2.4 T with gel, (*c*) B = 2.4 T without gel, (*d*) B = 0 T with gel, (*e*) B = 0 T without gel. The FWHM and FW10M widths are indicated by horizontal lines as a guide for the eye.

The angular separation of the peaks in the rocking curve is a measure of the relative misorientation of the crystallites. The broad profile of the single-peaked curve in Fig. 3(*e*) can be understood as the envelope function of a continuous distribution of small peaks (mosaic blocks).

In general, the mosaicity values determined by means of rocking-curve measurements are systematically smaller than those derived by standard integration software packages (Kabsch, 2001; Otwinowski & Minor, 1997). In general the latter incorporate the effects of not only crystal imperfection, but also of beam divergence and wavelength spread, which are substantial, especially for beamlines with focusing optics. Basically, these values are a measure of the angular integration box widths used by the data-processing software. In contrast, rocking-curve measurements of mosaicity more directly reflect a property of the sample. In general, the measurable rocking-width values are given by a convolution of the sample's 'true' mosaicity profile with the instrumental resolution function (Colapietro *et al.*, 1992) and thus have a lower limit imposed only by the remaining beam divergence and wavelength spread and, fundamentally, by the theoretical Darwin width of a reflection. In other words, for a perfect crystal with zero mosaicity, one would measure a rocking width given by the divergence (and wavelength spread) of the incident beam. For a perfect crystal and a (hypothetical) perfectly parallel and monochromatic beam, one would find a rocking width identical to the theoretical Darwin width, which can be calculated by the dynamical theory of X-ray diffraction (Helliwell, 1988; Authier, 2001). In the more realistic case of imperfect crystals and divergent beams, all effects superimpose and the experimentally measurable width $w_{\rm exp}$ is given in terms of the sample mosaicity η, the incident beam divergence δ_x, the wavelength spread $\Delta\lambda/\lambda$, the Bragg angle $\theta_{\rm B}$ and the Darwin width $w_{\rm D}$ by the relation

$$w_{\rm exp}^2 = \eta^2 + \delta_x^2 + \left(\frac{\Delta\lambda}{\lambda}\right)^2 \tan^2\theta_{\rm B} + w_{\rm D}^2. \qquad (1)$$

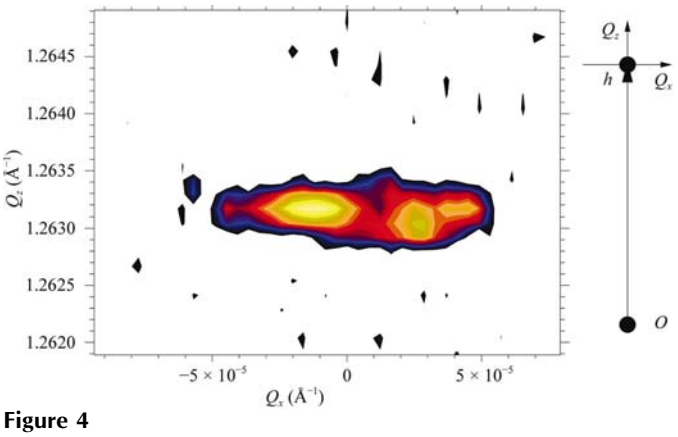

Figure 4
Reciprocal-space map, measured with an additional two-bounce Si(113) analyzer crystal, of the (776) reflection of a lysozyme crystal. As visible from the peak width along Q_z, lattice-parameter variations in the protein crystal do not exceed the level $\Delta d/d = 2\times10^{-4}$. For further explanations see main text. The sketch on the right shows the definition of the axes: Q_z along the diffraction vector (from the origin of reciprocal space O to the reciprocal-lattice point h) and Q_x perpendicular to it.

For our instrumental setup we have $\delta_x = 0.00032^\circ$, $(\Delta\lambda/\lambda)\tan\theta_{\rm B} = 0.00008^\circ$ and $w_{\rm D} \simeq 0.00001^\circ$. The cumulative effect of these instrumental contributions to the measured rocking widths accounts for only about 10% of the smallest measured FWHM values of 0.0007° and for less than 1% of the experimental width in the case of typical FWHM values larger than 0.002°. For this reason, the experimental widths will be interpreted directly in terms of crystal mosaicity for the rest of this article.

A potential alternative cause of peak broadening needs to be considered here. Potential lattice-parameter differences $\Delta d/d$ would also lead to peak broadening and cannot be distinguished from mosaicity by simple rocking-curve measurements. The two effects can only be differentiated by inserting an additional analyzer crystal into the exit beam path, acting as a collimator for the diffracted beam, and recording a two-dimensional reciprocal-space map (RSM; see Fig. 4). When plotted as a function of the two scattering-vector components Q_x and Q_z perpendicular and parallel to the reciprocal-lattice vector, respectively, mosaicity appears in this kind of map as a broadening of the Bragg peak along the horizontal direction (Q_x), whereas lattice-parameter variations lead to broadening along the vertical (Q_z) direction.

An experimental reciprocal-space map recorded for one sample from the series (grown without magnetic field and gel) is shown in Fig. 4. The visible broadening along Q_x contains the mosaicity information. The width along Q_z, on the other hand, is very narrow and allows the estimation of an upper limit for lattice-parameter variations in the sample of $\Delta d/d \leq 2\times10^{-4}$. Although reciprocal-space maps from other samples were not recorded owing to limited beamtime, it seems reasonable to assume that $\Delta d/d$ was comparably small for all samples grown under similar conditions. Even so, it needs to be kept in mind when interpreting rocking-curve widths in terms of sample properties that a certain contribution to the width may arise from lattice-parameter variations rather than mosaicity. In our case, this contribution amounts to a maximum of $\Delta\omega = \tan\theta_{\rm B}(\Delta d/d) = 0.0009^\circ$.

Fig. 5 shows three rocking curves measured from the same crystal for the same reflection but at different azimuth (Ψ) angles. While two of the curves show side peaks, the third curve only has one single narrow peak. Clearly, the misoriented crystallites that gave rise to the side peaks are still present in the sample, but in the special geometry of this third measurement their intensity signal coincides with the main peak. In other words, a single narrow rocking curve is no definitive proof of the absence of misoriented crystallites; their signal may just happen to be superposed on the main peak in a special measurement geometry. Only after recording a series of curves at different azimuth angles can one conclude from narrow widths that there is high crystalline perfection.

Similarly, Fig. 6 shows rocking curves from four different reflections of the same crystal. While the upper two are rather broad, the (776) and in particular the (008) reflection have very small mosaicities. This demonstrates that crystal mosaicity can be highly anisotropic. In order to obtain representative values of a crystal's mosaicity, measurements along at

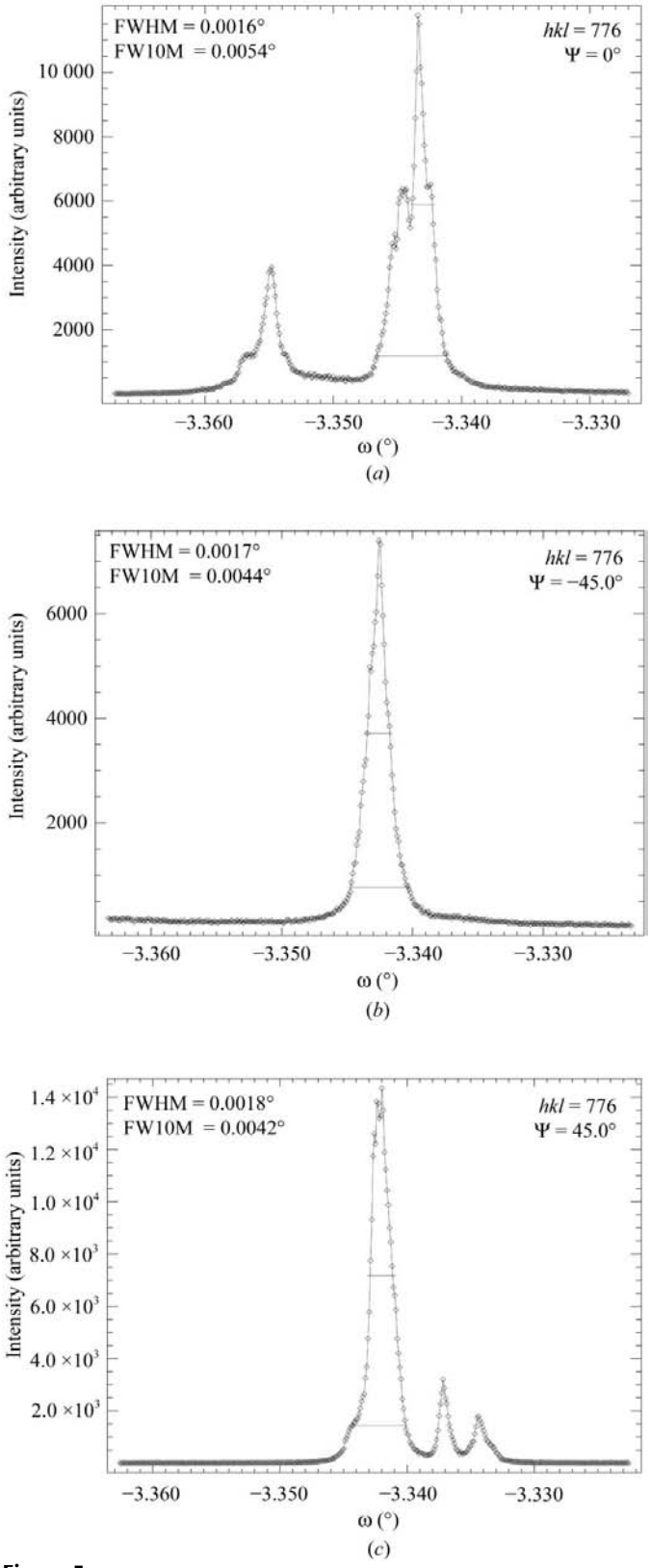

Figure 5
Rocking curves measured in different azimuth (Ψ angle) positions of the (776) reflection of one lysozyme crystal grown with gel and in a magnetic field. The considerable differences in shape and width of these curves show the anisotropic nature of the crystal's mosaicity along different directions in reciprocal space, even for the same reflection. The Ψ values are given with respect to an arbitrary reference.

least three non-coplanar directions of reciprocal space are required.

Together with the findings from Fig. 5, we conclude that it is by no means sufficient to carry out only one single measurement per crystal. When aiming to compare different crystal-growth methods, it is crucial to systematically record series of rocking curves at several different reflections and azimuth angles per crystal and to compare not single pairs of widths but the full series of width values thus obtained in order to obtain statistically significant results.

Two different ways of determining the width of many measured profiles by automated computer calculation are sketched in the curves of Fig. 3. The most obvious choice, the width at 50% of the maximum intensity (FWHM), is sufficient to completely characterize the shape of an ideal Gaussian profile. It may be misleading, however, in the case of double or multiple peaks, since it only takes into account the width of the main peak and often completely ignores intensity in the side peaks and the tails of the curve. Therefore, the curve widths were numerically analyzed in two alternative ways. The full width at 10% of the maximum intensity (FW10M) yields a more representative measure of the curve widths in many cases and is shown in Fig. 3 along with the FWHM. The noise level in the tails of all measured curves was clearly below the 10% level, facilitating reliable numerical determination of the FW10M value. As visible from the lower left curve, this measure of curve width does fail in occasional cases of side peaks separated from the main peak by valleys which drop below 10% of the maximum intensity. In order to also obtain a reliable criterion for these cases, the following third definition of width was used: $\sigma(w) = [\sum_i I(\omega_i)(\omega_i - \bar{\omega})^2 / \sum_i I(\omega_i)]^{1/2}$, where $\bar{\omega}$ is the centre of mass of the distribution: $\bar{\omega} = \sum_i I(\omega_i)\omega_i / \sum_i I(\omega_i)$. The width $\sigma(\omega)$ is just the standard deviation of the angular orientation distribution of the ensemble of mosaic blocks. In the following, we will abbreviate it as the 'variance' width. It is a measure of the fluctuation of the intensity distribution around its centre and is much more sensitive to intensity in well separated side peaks than the FWHM and FW10M.

4. Statistical analysis and discussion

In order to analyze the effect of various factors on crystal mosaicity at a better level of statistical significance, we will use in the following the width measures determined from the whole set of 263 experimental rocking curves. We analyze the effect of crystal-growth conditions (gel and magnetic field) by histograms of width values subdivided into four categories, as shown in Fig. 7. The number of crystals and of measurements contributing to each plot can be found from Tables 1 and 2.

From the graphs of FWHM values in Fig. 7, it is apparent that samples grown with gel and magnetic field (lower right plot) have a slightly lower overall mosaicity than those grown without gel and magnetic field (upper left plot). The effect is rather small, however, and cannot easily be analyzed in terms of the individual influences of gel and magnetic field. The comparison of the left and right columns and of the upper and

lower rows, respectively, does not show very clear trends. This is partly because of the rather small number of crystals contributing to each plot (see Table 1); the lower left plot in particular suffers from limited statistics. This is particularly true when considering that the nine highest FWHM values contained in this graph all originate from the same sample. To obtain more significant results from this type of comparison, one would therefore need to measure a considerably larger number of crystals.

A similar plot of FW10M rather than FWHM values (Fig. 8) shows a slightly clearer trend, in particular for the influence of the magnetic field in samples grown without gel. If we assume that the difference in FW10M and FWHM owing to the magnetic field is significant, then the main volume of the crystal lattice is not altered by the magnetic field, but the tendency for small outlier crystallites to deviate from the majority orientation is (slightly) reduced by the influence of the magnetic field.

In the case of the third measure of curve widths, the 'variance' width defined above (Fig. 9), effects of both the magnetic field and gel are more evident. As stated above, this width measure is more sensitive to intensity contributions further away from the centre of the intensity distribution in the rocking curve and is influenced especially strongly by split peaks or side peaks that are well separated from the main peak. Our result therefore means that both the magnetic field and the gel do not affect the growth of the main volume of the tetragonal lysozyme crystals, but can reduce or partially prevent the formation or growth of well separated and misoriented small outlier crystallites.

To analyze the effect of both factors in these plots more precisely than is possible by mere visual inspection, it appears desirable to quantify their influence by some statistical procedure. A statistical hypothesis test would typically assume some analytical distribution function for the envelope of the histograms. The hypothesis that any two experimental distributions differ significantly could then be tested by first assuming that they are drawn from the identical random distribution function and then calculating the *a priori* probability that their centres are shifted by the value found from

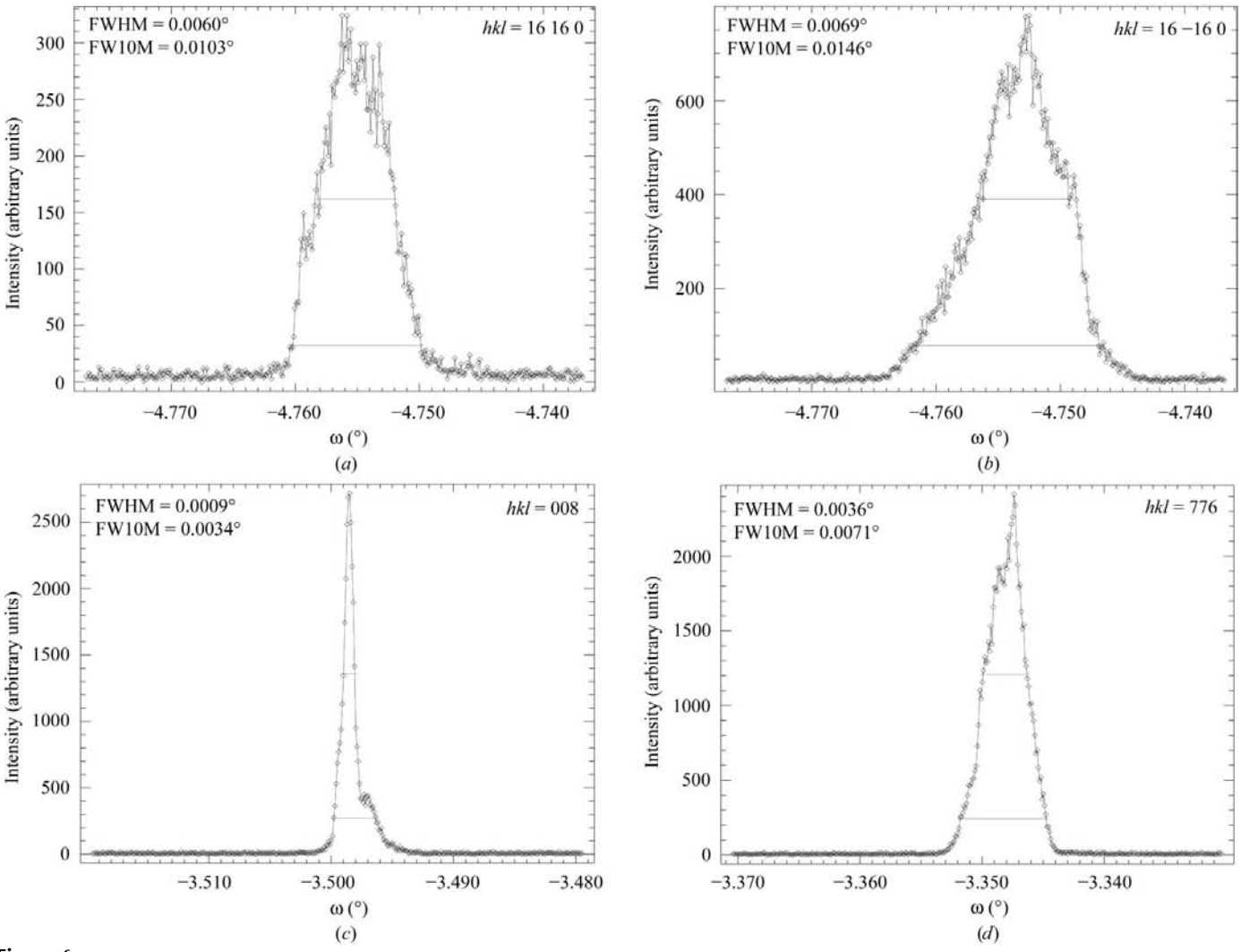

Figure 6
Rocking curves measured at four different reflections of the same crystal, grown without gel and without magnetic field. The considerable difference in the widths of these curves indicates a strong dependence of crystal mosaicity on the direction in reciprocal space (*i.e.* an anisotropic mosaicity).

the experimental distributions. If this probability (termed the *P* value) turns out to be lower than a selected fixed significance level (mostly chosen to be 5 or 1%), the assumption of identical distributions is statistically falsified and a significant effect is demonstrated. Application of this recipe to our histogram data is hindered at first by the lack of an obvious model for the envelope function of the experimental histograms (the individual mosaicity distributions). However, there is one kind of test in the statistical literature that works without assuming an explicit distribution function, the Wilcoxon rank-sum test (see, for example, Stahel, 2002). It can be performed by combining all values from both data sets into one common vector of values, sorting them in increasing order and determining the positions of the single entries within this combined array (their ranks). By summing the ranks of all entries separately for the two categories of data involved and normalizing appropriately, a test value is obtained that is known to be approximately distributed as a Gaussian, and *P* values can be easily determined from tables of the integrated normal distribution.

By applying this hypothesis test to the data in Figs. 7, 8 and 9 we obtain the *P* values given in Table 3. The results show that the influence of the magnetic field on crystal mosaicity is significant at the 5% level (or even at the 1% level) only when analysing the rocking-curve widths in terms of the 'variance' width (third row of Table 3). The data for the FWHM and the FW10M widths indicate a significant effect on crystal quality of growth in gel (in all four cases, with and without magnetic field), but not of growth in a magnetic field (only in one of the four cases). This confirms quantitatively the main features already discussed above on a more qualitative level.

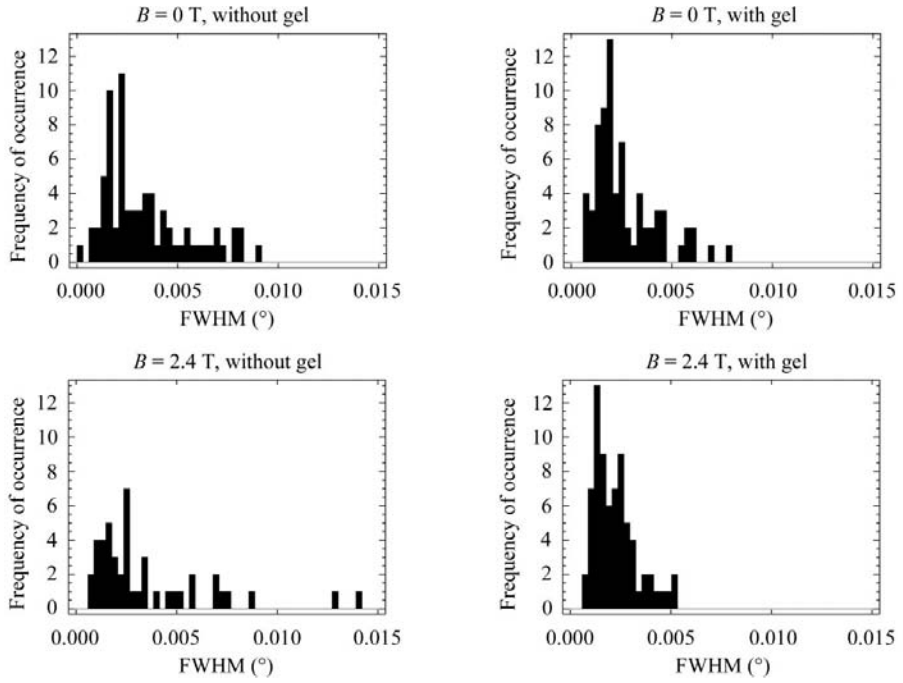

Figure 7
Histograms of FWHM values calculated separately for samples grown under four different conditions. Note that both the *x* and *y* scales are identical in all four graphs.

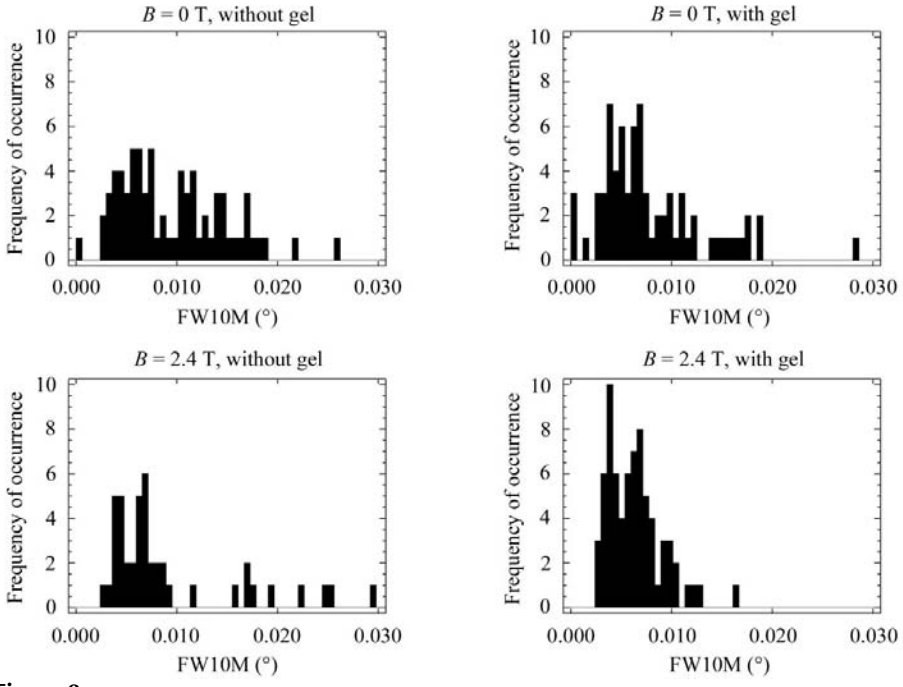

Figure 8
Histograms of full width at 10% maximum height (FW10M) values calculated separately for samples grown under four different conditions.

5. Determination of mosaicity and grain structure in real-space: rocking-curve imaging

Standard rocking-curve measurements can reveal the relative angular (mis-) orientation of mosaic blocks in a crystal. However, the spatial distribution of mosaic blocks inside the crystal can only be determined by techniques which provide additional spatial resolution. X-ray diffraction topography is a classical technique with widespread use in investigations of semiconductor crystals (for an overview see, for example, Bowen & Tanner, 1998) and has been transferred successfully to protein crystals in a number of studies (Fourme *et al.*, 1995; Stojanoff *et al.*, 1997; Lorber *et al.*, 1999; Otalora *et al.*, 1999). More recently, several groups have made combined use of X-ray

topography and reciprocal-space mapping techniques to characterize macromolecular crystals (Boggon *et al.*, 2000; Volz & Matyi, 2000; Hu *et al.*, 2001).

A combination of rocking-curve measurements with digital X-ray topography, termed rocking-curve imaging (RCI) and originally developed for the study of semiconductor substrate wafers (Lübbert *et al.*, 2000; Mikulík *et al.*, 2003), allows the determination of quantitative information on the angular misorientation and the spatial arrangement of mosaic blocks as well as the distribution of lattice quality and defects within a crystal. The application of the technique to protein crystals is not straightforward, mainly owing to their lower scattering power, small size, the initially unknown orientation of their crystal axes and their sensitivity to radiation damage. It will be shown here that in spite of these difficulties the technique can be successfully transferred to protein crystals and yields promising results.

Rocking-curve imaging realises spatial resolution in the diffracted beam by using an X-ray sensitive digital CCD camera rather than a point detector or X-ray film. The camera used for the present study had a nominal pixel size of 5 μm, giving about 13 μm actual spatial resolution. The spatial intensity profile of the diffracted beam is recorded at a series of angular positions along the sample's rocking curve, yielding a sequence of digital X-ray topographs. The series of images can be rearranged to obtain a two-dimensional array of rocking curves, one for each position on the sample. By pixel-wise analysis of the shapes of these curves in terms of peak positions, intensities and widths, the spatial variation of crystal quality across the sample can be visualized.

Selected single topographs from a lysozyme crystal grown without gel and magnetic field are shown in Fig. 10. Fig. 11 demonstrates that rocking curves obtained in this way from a series of images are indeed principally equivalent to the more traditional global rocking curve. By analyzing the full sequence of 40 images taken along the rocking curve with an angular step width of 0.00035°, we obtain a two-dimensional array of rocking-curve widths which can again be visualized as an image with the same spatial dimensions as the original topographs (see Fig. 12).

The main features of Fig. 12 are a zone of relatively large rocking-curve widths (lower crystalline perfection) at the centre of the sample, surrounded by zones of very narrow widths indicating a highly regular crystal lattice. A possible interpretation of these data is that the centre corresponds to a nucleation zone where crystal growth started and that the lattice progressively grew more homogeneous when growth continued to the outer zones, although of course the image shows only a two-dimensional projection (along the exit-beam direction) of the three-dimensional crystal volume. As above for the global rocking curves, the favoured interpretation of larger widths of such local rocking curves is in terms of increased mosaicity. The population of microcrystallites at the centre of the crystal shows a wider distribution of orientations than those at the edges. However, we cannot presently rule out the possibility that a contribution to the larger widths derives from strain

Table 3
P values resulting from the application of Wilcoxon's rank-sum test (see main text) to test whether the mosaicity distributions in Figs. 7–9 differ in a statistically significant way.

The first data column in this table (comparison of growth with and without gel, both at $B = 0$ T) is the result of comparing the upper left with the upper right histogram in each of the plots. Similarly, the second data column results from comparing the lower left and the lower right histogram, the third column from comparing the upper left and the lower left histogram *etc*. The first, second and third data rows in this table concern Figs. 7, 8 and 9, respectively. A statistically significant change in mosaicity is indicated by a *P* value lower than a given significance threshold. Setting this level to 0.05, the effect of growth in gel is significant in all cases except one, whereas growth in a magnetic field leads to significant reduction of mosaicities only in three of six cases. It is most evident for the 'variance' measure of width. See main text for further discussion.

Comparison of with	No gel, $B = 0$ T Gel, $B = 0$ T	No gel, $B = 2.4$ T Gel, $B = 2.4$ T	No gel, $B = 0.0$ T No gel, $B = 2.4$ T	Gel, $B = 0.0$ T Gel, $B = 2.4$ T
FWHM	0.0213	0.0097	0.4524	0.0774
FW10M	0.0323	0.0142	0.2331	0.0208
'Variance' width	0.0001	0.0862	0.0000	0.0000

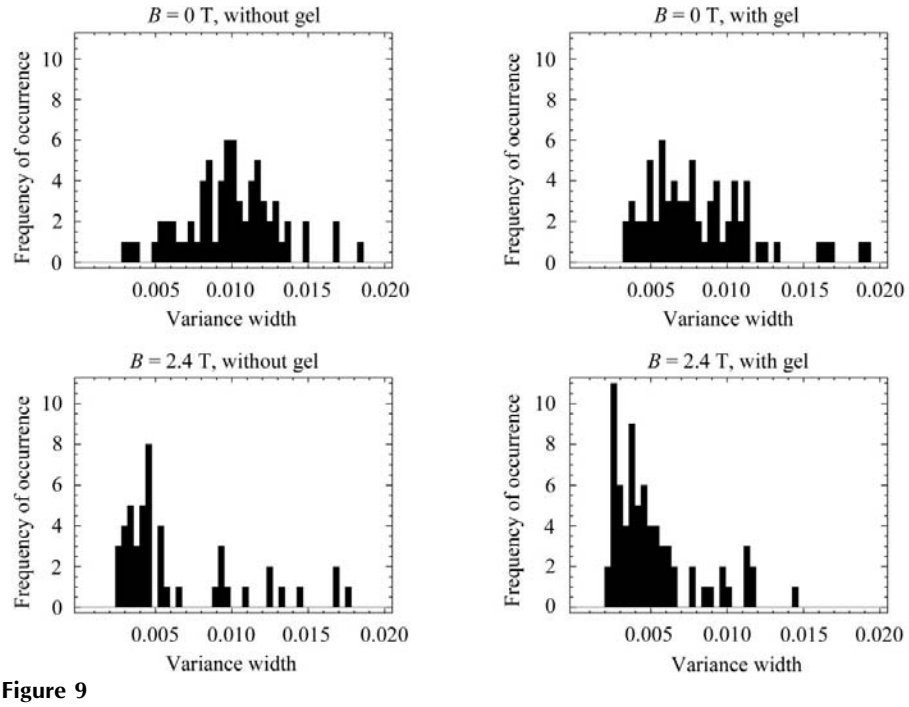

Figure 9
Histograms of 'variance' width values, calculated separately for samples grown under four different conditions.

effects, *i.e.* that the centre of the crystal shows slightly larger lattice-parameter variations than the outer regions. In this case, the additional divergence of the exit beam caused by variations in local Bragg angles would lead to a blurring of the image on the CCD camera. This effect can be calculated from the knowledge of the maximum Bragg angle difference and the sample-to-detector distance. Its importance can be minimized by placing the camera very close to the sample; even for the relatively large distance used in this experiment (65 cm) it amounts to a maximum of 16 μm, *i.e.* close to one resolution element (13 μm) of the camera only.

The results of this first application of the rocking-curve imaging technique are to be considered as preliminary and will be complemented by similar studies on larger numbers of samples. Also, by investigating several different reflections per sample, it may be possible in the future to obtain a true three-dimensional picture of lattice misorientations. At present, our results demonstrate that the technical challenges can be overcome, that the spatial distribution of mosaicity and crystal quality can indeed be imaged even in macromolecular crystals and that the field of topography studies of proteins can be made to benefit from the advantages of digital imaging and data analysis.

6. Conclusion

In summary, we have shown how accurate X-ray diffraction rocking-curve measurements can be used to assess the detailed mosaicity of protein crystals. A high-resolution setup, including an X-ray beam with low divergence and low wavelength spread as well as a highly precise diffractometer, was crucial to achieving the required angular resolution. The resulting mosaicity values were very low, close to the lower limit imposed by the beam divergence and the theoretical Darwin width, demonstrating the generally very good lattice quality and homogeneity achievable for lysozyme crystals.

Results of comparing histograms of mosaicity values from a number of protein crystals grown under different conditions are compatible with the hypothesis that crystal growth both in gel and in a homogeneous magnetic field of 2.4 T can improve crystal quality. The effect is very small, however, in the case of lysozyme grown in a field of 2.4 T. While the average rocking-curve FWHM does not change significantly upon application of the magnetic field during growth, other width measures (the FW10M and the 'variance' width) do show a slight decrease. Thus, although the orientation distribution of the majority of crystallites does not become narrower, the tendency of small outlier crystallites to diverge from the predominant orienta-

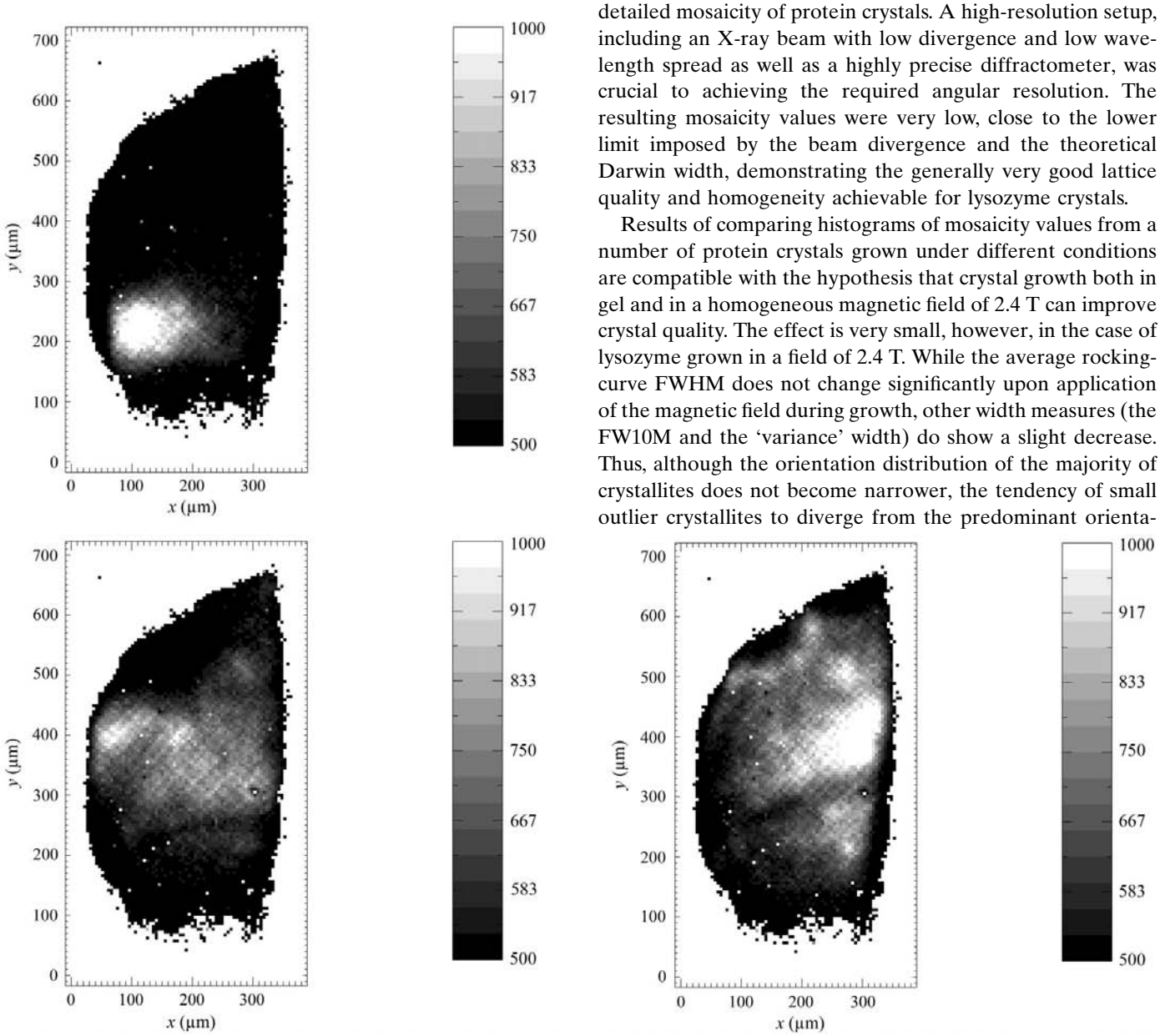

Figure 10
Examples of digital topographs recorded on the (776) reflection of a lysozyme crystal grown without gel and magnetic field. The images are extracted from the full series of 40 digital topographs recorded at different rotation angles along the rocking curve of the sample. The bars on the right define the colour scale used for plotting the intensity values (in units of counts per pixel). Relative angular positions $\omega = -0.0025$ (top), 0.000 (bottom left) and $+0.0014^{\circ}$ (bottom right).

tion may be reduced owing to the action of the magnetic field. Since the quality of all tetragonal lysozyme crystals was already very good, we do not anticipate any significant influence of the investigated growth conditions on the resolution limit achievable in an intensity data collection.

These results, if confirmed more clearly on even larger numbers of samples, may be interpreted as experimental evidence supporting theories by Lin *et al.* (2000). More unambiguous information on the effect of homogeneous magnetic fields on protein crystal quality may be expected from studies at higher magnetic fields. Also, the case of the model protein lysozyme is not representative in that the crystallization conditions are very well known and a relatively good crystal quality can be achieved with standard growth methods. Crystallization experiments with other proteins and higher magnetic fields are under way.

To complement our mosaicity study, we have introduced the rocking-curve imaging method to monitor the grain structure and the distribution of crystallite misorientation in real space. A first application to proteins indicated that this method can indeed be extended to macromolecular crystals. Informative digital topographs can be recorded and the power of digital data analysis can be exploited to obtain a wealth of information from a large set of local rocking curves. The results from a tetragonal lysozyme crystal may be interpreted as showing a disturbed nucleation zone with higher mosaicities (or *d*-spacing differences) at the centre, surrounded by a more perfect outer crystal area. Spatially resolved crystal-quality information of this kind may prove useful to trace back the growth history and the formation of defects in protein crystal growth.

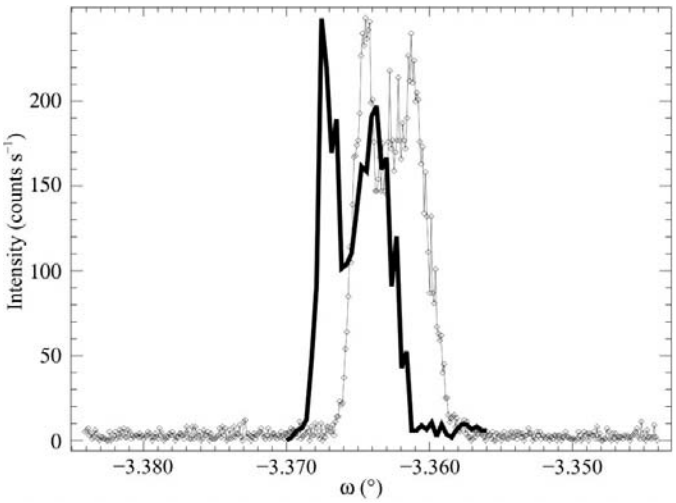

Figure 11
Comparison of the global rocking curve measured with a point detector (thin line with diamond symbols) with a curve reconstructed from the series of images in Fig. 10 by summation of all individual local rocking curves (thick line). The two curves agree well, apart from an overall angular shift which may arise from a slight slipping of the crystal between measurements.

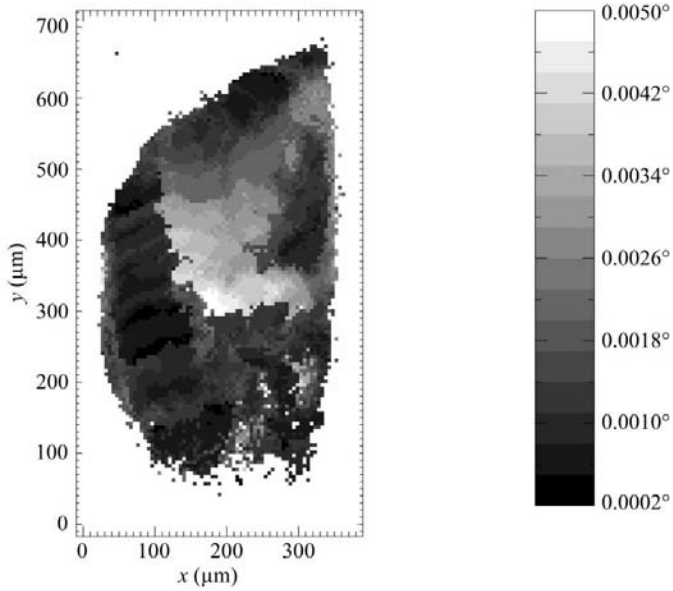

Figure 12
Map of local rocking-curve half widths (°) calculated from the series of single topograms (see Fig. 10) by pixel-wise analysis of rocking-curve shapes (for details, see main text). The map shows a zone of larger rocking-curve half-widths at the center of the crystal, surrounded by areas of narrower rocking curves. The bar on the right defines the color scale used for plotting the local width values.

We would like to thank Hermann Franz for help in setting up and aligning the beamline and Anita Ehnes for initial technical assistance.

References

Astier, J. P., Veesler, S. & Boistelle, R. (1998). *Acta Cryst.* D**54**, 703–706.
Ataka, M., Katoh, E. & Wakayama, N. I. (1997). *J. Cryst. Growth*, **173**, 592–596.
Ataka, M. & Wakayama, N. I. (2002). *Acta Cryst.* D**58**, 1708–1710.
Authier, A. (2001). *Dynamical Theory of X-ray Diffraction.* Oxford University Press.
Bellamy, H. D., Snell, E. H., Lovelace, J., Pokross, M. & Borgstahl, G. E. O. (2000). *Acta Cryst.* D**56**, 986–995.
Biertümpfel, C., Basquin, J., Suck, D. & Sauter, C. (2002). *Acta Cryst.* D**58**, 1657–1659.
Boggon, T. J., Helliwell, J. R., Judge, R. A., Olczak, A., Siddons, D. P., Snell, E. H. & Stojanoff, V. (2000). *Acta Cryst.* D**56**, 868–880.
Borgstahl, G. E. O., Vahedi-Faridi, A., Lovelace, J., Bellamy, H. D. & Snell, E. H. (2001). *Acta Cryst.* D**57**, 1204–1207.
Bowen, D. K. & Tanner, B. K. (1998). *High Resolution X-ray Diffractometry and Topography.* London: Taylor & Francis.
Colapietro, M., Cappuccio, G., Marciante, C., Pifferi, A., Spagna, R. & Helliwell, J. R. (1992). *J. Appl. Cryst.* **25**, 192–194.
Cudney, R., Patel, S. & McPherson, A. (1994). *Acta Cryst.* D**50**, 479–483.
Dong, J., Boggon, T. J., Chayen, N. E., Raftery, J., Bi, R.-C. & Helliwell, J. R. (1999). *Acta Cryst.* D**55**, 745–752.
Fourme, R., Ducruix, A., Riès-Kautt, M. & Capelle, B. (1995). *J. Synchrotron Rad.* **2**, 136–142.
Garcia-Ruiz, J. M., Gonzalez-Ramirez, L. A., Gavira, J. A. & Otálora, F. (2002). *Acta Cryst.* D**58**, 1638–1642.
Garcia-Ruiz, J. M. & Moreno, A. (1994). *Acta Cryst.* D**50**, 484–490.
Helliwell, J. R. (1988). *J. Cryst. Growth*, **90**, 259–272.
Henisch, H. (1988). *Crystal Growth in Gels and Liesegang Rings.* Cambridge University Press.

Hu, Z. W., Thomas, B. R. & Chernov, A. A. (2001). *Acta Cryst.* D**57**, 840–846.
Kabsch, W. (2001). *International Tables for Crystallography*, Vol. *F*, edited by M. Rossmann & E. Arnold, ch. 25.2.9. Dordrecht: Kluwer Academic Publishers.
Lin, S.-X., Zhou, M., Azzi, A., Xu, G.-J., Wakayama, N. & Ataka, M. (2000). *Biochem. Biophys. Res. Commun.* **275**, 274–278.
López-Jaramillo, F. J., Garciá-Ruiz, J. M., Gavira, J. A. & Otálora, F. (2001). *J. Appl. Cryst.* **34**, 365–370.
Lorber, B., Sauter, C., Ng, J., Zhu, D., Giegé, R., Vidal, O., Robert, M. & Capelle, B. (1999). *J. Cryst. Growth*, **204**, 357–368.
Lübbert, D., Baumbach, T., Härtwig, J., Boller, E. & Pernot, E. (2000). *Nucl. Instrum. Methods B*, **160**, 521–527.
Meents, A., Lübbert, D., Franz, H. & Weckert, E. (2004). In preparation.
Mikulík, P., Lübbert, D., Korytár, D., Pernot, P. & Baumbach, T. (2003). *J. Phys. D: Appl. Phys.* **36**, A74–A78.
Miller, T. Y., He, X. & Carter, D. C. (1992). *J. Cryst. Growth*, **122**, 306–309.
Otalora, F., Garcia-Riuz, J. M., Gavira, J. A. & Capelle, B. (1999). *J. Cryst. Growth*, **196**, 546–558.
Otwinowski, Z. & Minor, W. (1997). *Methods Enzymol.* **276**, 307–326.
Pauling, L. (1936). *J. Chem. Phys.* **4**, 673–677.
Provost, K. & Robert, M.-C. (1991). *J. Cryst. Growth*, **110**, 258–264.
Qi, J., Wakayama, N. I. & Ataka, M. (2001). *J. Cryst. Growth*, **232**, 132–137.
Qi, J., Wakayama, N. I. & Yabe, A. (1999). *J. Cryst. Growth*, **204**, 408–412.
Robert, M. & Lefaucheux, F. (1988). *J. Cryst. Growth*, **90**, 358–367.
Sakurazawa, S., Kubota, T. & Ataka, M. (1999). *J. Cryst. Growth*, **196**, 325–331.
Sato, T., Yamada, Y., Saijo, S., Hori, T., Hirose, R., Tanaka, N., Sazaki, G., Nakajima, K., Igarashi, N., Tanaka, M. & Matsuura, Y. (2001). *J. Cryst. Growth*, **232**, 229–236.
Sazaki, G., Yoshida, E., Komatsu, H., Nakada, T., Miyashita, S. & Watanabe, K. (1997). *J. Cryst. Growth*, **173**, 231–234.
Snell, E. H., Cassetta, A., Helliwell, J. R., Boggon, T. J., Chayen, N. E., Weckert, E., Hölzer, K., Schroer, K., Gordon, E. J. & Zagalsky, P. F. (1997). *Acta Cryst.* D**53**, 231–239.
Snell, E. H., Weisgerber, S., Helliwell, J. R., Weckert, E., Hölzer, K. & Schroer, K. (1995). *Acta Cryst.* D**51**, 1099–1102.
Stahel, W. A. (2002). *Statistische Datenanalyse*, 4th ed. Wiesbaden: Vieweg Verlag.
Stojanoff, V., Siddons, D. P., Monaco, L. A., Vekilov, P. & Rosenberger, F. (1997). *Acta Cryst.* D**53**, 588–595.
Thiessen, K. J. (1994). *Acta Cryst.* D**50**, 491–495.
Vidal, O., Robert, M., Arnoux, B. & Capelle, B. (1999). *J. Cryst. Growth*, **196**, 559–571.
Volz, H. M. & Matyi, R. J. (2000). *Acta Cryst.* D**56**, 881–889.
Wakayama, N. I., Ataka, M. & Abe, H. (1997). *J. Cryst. Growth*, **178**, 653–656.
Weckert, E. & Hümmer, K. (1997). *Acta Cryst.* A**53**, 108–143.
Worcester, D. (1978). *Proc. Natl Acad. Sci. USA*, **75**, 5475–5477.
Yanagiya, S., Sazaki, G., Durbin, S. D., Miyashita, S., Nakada, T., Komatsu, H., Watanabe, K. & Motokawa, M. (1999). *J. Cryst. Growth*, **196**, 319–324.
Yanagiya, S., Sazaki, G., Durbin, S. D., Miyashita, S., Nakajima, K., Komatsu, H., Watanabe, K. & Motokawa, M. (2000). *J. Cryst. Growth*, **208**, 645–650.
Yin, D. C., Inatomi, Y., Wakayama, N. I., Huang, W. D. & Kuribayashi, K. (2002). *Acta Cryst.* D**58**, 2024–2030.
Zhong, C. & Wakayama, N. I. (2001). *J. Cryst. Growth*, **226**, 327–332.
Zhu, D.-W., Lorber, B., Sauter, C., Ng, J. D., Bénas, P., Le Grimellec, C. & Giegé, R. (2001). *Acta Cryst.* D**57**, 552–558.